scientific reports

Check for updates

OPEN

Mannose-B from *Codonopsis pilosula* modulates LAMB1 expression to enhance trophoblast function and alleviate subchorionic hematoma

Qian Sun[1,2,3,10], Yuan Gao[1,10], Kadirya Asan[3,10], Jing Ji[3], Jinjin Xu[1], Xiaoyan Wu[1,2], Jie Ren[1], Wen Feng[1], Mengwei Song[3], Sen Wang[3], Boyu Zhang[3], Ying Zhou[3], Conghui Han[4,5,6,7]✉, Shun Liu[8]✉ & Wen Yang[1,2]✉

This study investigates the active component Mannose-B from *Codonopsis pilosula* and its effect on human trophoblast cell function, particularly focusing on the regulation of Laminin Subunit Beta 1 (LAMB1) expression and its implications in subchorionic hematoma (SCH). Key genes involved in SCH pathology were identified through RNA sequencing and bioinformatics analysis. Network pharmacology was utilized to screen active components in *Codonopsis pilosula* and their critical targets. In vitro, HTR-8/Svneo cells were used to assess proliferation, migration, and invasion through CCK8, Transwell, and cell migration assays. A SCH rat model was established to evaluate changes in coagulation parameters, litter size, fetal viability, and fetal and placental weights. In vivo validation of Mannose-B's effects on LAMB1 expression and SCH pathology was performed using RT-qPCR and Western Blot. Network pharmacology and molecular docking identified Mannose-B as a potentially active compound in *Codonopsis pilosula*, with LAMB1 as a significant predicted target. In vitro experiments suggested that Mannose-B may promote HTR-8/Svneo cell proliferation, migration, and invasion by downregulating LAMB1 expression. In vivo experiments showed a reduction in placental LAMB1 expression and partial improvement in SCH-related pathological features. Mannose-B from *Codonopsis pilosula* may alleviate SCH progression by modulating LAMB1 expression and enhancing trophoblast cell function. However, these findings remain preliminary and require further investigation to confirm the underlying mechanisms and clinical relevance.

Keywords Subchorionic hematoma, *Codonopsis pilosula*, Mannose-B, Laminin subunit beta 1, Trophoblast cells, Network pharmacology

Subchorionic hematoma (SCH) is a common and significant pathological condition during pregnancy, characterized by the accumulation of blood beneath the uterine endometrium. This pathology not only amplifies anxiety and discomfort in pregnant women but also can substantially impact pregnancy outcomes, leading to complications such as miscarriage, preterm birth, and fetal growth restriction[1–3]. Current research indicates that abnormal functionality of the trophoblast cells, specifically weakened migration and invasion capabilities, serves as a pivotal factor in the development of SCH[4]. Trophoblast cells play a vital role in the formation of the placenta, and any dysfunction directly affects placental development, consequently influencing fetal health[5].

[1]Department of Gynecology, The first people's hospital of Lianyungang, Lianyungang 222061, China. [2]The first affiliated hospital of Kangda College of Nanjing Medical University, Lianyungang 222061, China. [3]Jiangsu Key Laboratory of Marine Pharmaceutical Compound Screening, College of Pharmacy, Jiangsu Ocean University, Lianyungang 222000, China. [4]Department of Urology, Xuzhou Clinical School of Xuzhou Medical University, Jiangsu, China. [5]Department of Urology, Xuzhou Central Hospital, Xuzhou, Jiangsu, China. [6]School of Life Sciences, Jiangsu Normal University, Jiangsu, China. [7]Department of Urology, Heilongjiang Provincial Hospital, Huaibei, Heilongjiang, China. [8]Kangda College of Nanjing Medical University, No. 88, Chunhui Road, Huagoshan Avenue, Haizhou District, Lianyungang 222000, Jiangsu Province, China. [10]Qian Sun, Yuan Gao and Kadirya Asan These authors are regarded as co-first authors. ✉email: hanconghuidoctor@vip.qq.com; lsadcy@163.com; wen_yang0@163.com

Despite certain advancements in the clinical diagnosis and management of SCH, a deeper understanding of its pathogenesis remains essential. Therefore, exploring the pathological mechanisms of SCH holds critical clinical significance for its prevention and treatment.

Codonopsis pilosula, known as Dang Shen in traditional Chinese medicine (TCM), is widely utilized for nourishing qi and blood, as well as enhancing immunity[6–8]. Recent pharmacological studies have revealed that *Codonopsis pilosula* contains various bioactive components such as polysaccharides, saponins, and flavonoids, exhibiting pharmacological effects like anti-inflammatory, antioxidant, and immune-modulating properties[9,10]. Among these components, Mannose-B, a significant active ingredient in *Codonopsis pilosula*, has garnered scientific attention[11,12]. Studies have shown that Mannose-B regulates cell proliferation and differentiation, yet its specific mechanisms in pregnancy-related disorders, particularly in SCH, remain unclear[13]. Further research on *Codonopsis pilosula* and its active constituents can not only unveil the scientific basis of its traditional use but also provide novel insights for its modern medical applications.

Laminin Subunit Beta 1 (LAMB1), a crucial member of the laminin protein family, extensively participates in cell adhesion, migration, and tissue morphology formation. LAMB1 plays a critical role in the construction of the extracellular matrix, and alterations in its expression levels are closely associated with various disease states. For instance, in tumor biology, abnormal expression of LAMB1 is linked to tumor cell invasion and metastasis[14]. Similarly, during gestation, LAMB1 plays a critical role in establishing and sustaining the decidual microenvironment which is necessary for placental implantation and subsequent physiological functions[15,16]. Particularly in the pathological process of SCH, the overexpression of LAMB1 is considered one of the significant reasons for trophoblast cell dysfunction. Therefore, thorough investigation into the expression changes of LAMB1 in SCH and its regulatory mechanisms can aid in understanding the pathophysiological processes of SCH and offer potential targets for developing new therapeutic strategies.

To delve into the mechanism of action of the active component Mannose-B from *Codonopsis pilosula* in SCH, this study employed whole transcriptome sequencing technology and bioinformatics analysis to identify key genes associated with the SCH pathological process. Additionally, utilizing network pharmacology and molecular docking techniques, the study identified effective active components from *Codonopsis pilosula* that regulate SCH and their crucial targets. In vitro experiments were conducted using the HTR-8/Svneo human trophoblast cell line, where the impact of Mannose-B on cell proliferation, migration, and invasion was assessed through CCK8, Transwell, and cell migration assays. Furthermore, a SCH rat model was established to evaluate clotting parameters, litter size, fetal viability, fetal and placental weights among rat groups, confirming the role of Mannose-B in modulating LAMB1 expression and the SCH pathological state. RT-qPCR and Western Blot analyses were utilized to detect changes in gene and protein expression levels, providing molecular evidence for unraveling the mechanism of action of Mannose-B.

This research aimed to investigate the influence of the effective component Mannose-B from *Codonopsis pilosula* on the functional changes of human trophoblast cells, particularly its role in SCH development through LAMB1 regulation. Specifically, through in vivo and in vitro experiments, the study aims to comprehensively elucidate the effects of Mannose-B on trophoblast cell proliferation, migration, and invasion, as well as its regulatory effect on LAMB1 expression and the pathological state in the SCH rat model. These investigations seek to reveal the potential mechanisms of Mannose-B in SCH treatment, offering new theoretical basis. Moreover, the study anticipates providing novel therapeutic strategies for the clinical prevention and treatment of SCH, promoting the application of *Codonopsis pilosula* and its active components in modern medicine. The research outcomes are expected to deepen the understanding of the pathological mechanisms of SCH, facilitate the development of related therapeutic interventions, and hold significant scientific research value and clinical application prospects.

Materials and methods

Construction of Rat Models

All animal experiments in this study were conducted in accordance with the ARRIVE 2.0 guidelines (Animal Research: Reporting of In Vivo Experiments)[17] and strictly adhered to the animal welfare regulations of China. The experimental protocol was approved by the Jiangsu Ocean University Experimental Animal Ethics Committee (No. Jou2022121107). All procedures were designed to optimize animal welfare and minimize suffering throughout the study and All methods were carried out in accordance with relevant guidelines and regulations.

A total of 40 ten-week-old SPF-grade female Wistar rats (weighing approximately 250 g) and 23 male rats (weighing around 260 g) were housed for the study. All rats were purchased from Beijing Vital River Laboratory Animal Technology Co., Ltd. (Beijing, China) with the product number 219. They were kept in an environment maintained at 50–60% humidity, a temperature of 22–24 °C, and subjected to a 12-hour light-dark cycle with ad libitum access to food and water. After an acclimatization period, rats were co-housed in a ratio of 2:1 for females to males. Vaginal smears were collected the next day for examination. If numerous sperm cells were observed, it was considered successful mating, designated as gestational day 0. Eventually, 36 female rats with confirmed pregnancies were selected for further investigation.

The rats were randomly assigned to four groups: Normal group ($n=12$), Model group ($n=12$), Model + Mannose-B group ($n=12$), and Model + Mannose-B + oe-LAMB1 group ($n=12$). Starting from the 5th day postpartum, Mannose-B (ST1231, Beyotime, Shanghai, China) was administered every 3 days by gavage. A single dose of LPS (L8880, SolBio, Beijing, China) diluted to 0.2 μg/mL along with lentivirus oe-LAMB1 or its mock control at a dose of 10 μg/kg was injected via the tail vein[18,19]. Lentivirus oe-LAMB1 was constructed using lentiviral overexpression vector (LV4, GeneChem, Shanghai, China). The Model group received 400 μL saline + 1 mL LPS + mock, Model + Mannose-B group received 50 mg/kg Mannose-B + 1 mL LPS + mock, and Model + Mannose-B + oe-LAMB1 group received 50 mg/kg Mannose-B + 1 mL LPS + oe-LAMB1.

On gestational day 19, 12 rats from each group underwent cesarean section to collect placentas and arterial blood from the abdominal aorta. The number of fetal pups was recorded, and litter size, litter survival rate, and fetal weight were assessed. Placentas were weighed post-delivery and stored at −80 °C for further analysis. Additionally, 12 rats from the Normal and Model groups each underwent immediate removal of fetal membranes and umbilical cords following cesarean delivery, and placental tissues were rapidly frozen in liquid nitrogen and then transferred to −80 °C for subsequent RNA extraction and transcriptome sequencing analysis[20].

RNA extraction and sequencing

Total RNA was extracted from placental tissues of model group rats and normal group rats, with 6 samples collected per group. The total RNA was isolated using Trizol reagent (15596026, Invitrogen, Carlsbad, CA, USA) and its concentration and purity were determined using the Agilent 2100 Bioanalyzer (G2939B, Agilent, USA). Total RNA samples meeting the following criteria were selected for subsequent experiments: RNA integrity number (RIN) ≥ 7.0 and 28 S:18 S ratio ≥ 1.5.

Sequencing libraries were generated and sequenced by CapitalBio Technology (Beijing, China). A total of 5 μg of RNA was used for each sample. Briefly, the Ribo-Zero™ Magnetic Kit (MRZE706, Epicentre Technologies, Madison, WI, USA) was employed to deplete ribosomal RNA (rRNA) from total RNA. The NEB Next Ultra RNA Library Prep Kit (#E7775, NEB, USA) was utilized for Illumina library construction and sequencing. Subsequently, RNA was fragmented into approximately 300 bp (bp) fragments in NEB Next First Strand Synthesis Reaction Buffer (5×). The first cDNA strand was synthesized using reverse transcriptase primers and random primers, followed by the synthesis of the second cDNA strand in NEB Next Second Strand Synthesis Reaction Buffer with dUTP Mix (10×). End repair of cDNA fragments, including polyA tail addition and sequencing adapter ligation, was performed. After ligating Illumina sequencing adapters, the second strand of cDNA was digested using USER Enzyme (#M5508, NEB, USA) to construct strand-specific libraries. The library DNA was amplified, purified, and enriched via PCR. Subsequently, library identification was conducted using the Agilent 2100 system and quantification was performed using the KAPA Library Quantification Kit (KK4844, KAPA Biosystems). Finally, paired-end sequencing was carried out on the Illumina NextSeq CN500 sequencer, with an average sequencing depth of 50x.

Quality control of sequencing data and differential gene analysis

The quality of paired-end reads of the raw sequencing data was assessed using FastQC software version 0.11.8. Preprocessing of the raw data was conducted using Cutadapt software version 1.18, which involved the removal of Illumina sequencing adapters and poly(A) tail sequences. A Perl script was employed to eliminate reads with an N content exceeding 5%. The FASTX Toolkit software version 0.0.13 was utilized to extract reads with a base quality exceeding 20 representing at least 70% of the sequence length. BBMap software was used for repairing the paired-end sequences. Subsequently, the high-quality filtered read fragments were mapped to the Gencode-provided Rnor_6.0 reference genome using hisat2 software version 0.7.12. Differential gene expression analysis between the normal and SCH model samples was performed using the "Limma" package in R software, with a threshold of $|\log2FC| > 2$ and a p-value < 0.05 to select differentially expressed genes (DEGs). Principal component analysis (PCA) was conducted using the "prcomp" function in the "stats" package of R, a heatmap was generated using the "heatmap" package to visualize the expression of DEGs, volcano plots were created using the "ggplot2" package to display DEGs, Gene Ontology (GO) and Kyoto Encyclopedia of Genes and Genomes (KEGG) enrichment analyses were performed using the "clusterProfiler" package, gene set enrichment analysis was carried out using the "GSVA" package, and weighted gene co-expression network analysis (WGCNA) was performed using the "WGCNA" package.

Construction of WGCNA

In this section, R software and the following packages were utilized: matrixStats, Hmisc, foreach, doParallel, fastcluster, dynamicTreeCut, survival, and WGCNA. Initially, normal datasets were removed, and missing values were checked and outlier samples were eliminated. Subsequently, samples were clustered based on gene expression levels. Then, an unscaled network was constructed by selecting the power value of 11 based on the Pearson correlation coefficients between genes, considering the mean connectivity in the unscaled network fitting process and the unscaled network model. A distance matrix between genes was built according to the selected power and clustered, followed by calculation of the Topological Overlap Matrix (TOM) to measure the interconnectedness of genes with similar expression profiles within modules. Lastly, a dynamic hybrid cut method was employed to divide these genes into distinct modules, selecting the module with the highest correlation with mRNA. Afterwards, the VennDiagram package was utilized for Venn analysis to filter out key genes by taking the intersection of genes from this module and DEGs within the transcriptome.

Enrichment analysis of differential genes

We conducted GO and KEGG functional enrichment analysis on the candidate genes/proteins using the "ClusterProfiler" package in the R software. In the GO enrichment analysis, we examined the biological processes (BP), cellular components (CC), and molecular functions (MF), applying a significance threshold of $p < 0.05$ for selection. Additionally, we performed pathway enrichment and visualization. For the KEGG enrichment analysis, significance was set at $p < 0.05$, and we visualized the enriched pathways and genes, effectively distinguishing the differential enrichment pathways of the marker genes in different clusters.

SPR analysis

The binding assay based on surface plasmon resonance (SPR) technology was performed using the Biacore X100 instrument (GE Healthcare). The candidate proteins were immobilized on a CM5 sensor chip in 10 mM sodium

acetate buffer (pH 4.5) using a standard amide coupling procedure. A protein solution of 100 μg/ml was injected to react with the activated surface. The chip was equilibrated for 4 h at room temperature with 1.05x PBS buffer. After Mannose-B was diluted in gradients, it was injected at a flow rate of 30 μL/min for 60 s (contact phase), followed by 120 s of buffer flow (dissociation phase). KD values were calculated using BIAevaluation software (GE Healthcare).

Identification and screening of active chemical components and their target sites of radix codonopsis

A search for Radix Codonopsis in the SymMap database (http://www.symmap.org/) was conducted to identify its active chemical components. Compounds with Oral Bioavailability (OB) > 30% and Drug-likeness (DL) > 0.18 were selected as screening criteria to identify representative chemical components of Radix Codonopsis. Subsequently, compounds without target sites or redundant active ingredients were excluded for further analysis.

Construction of the" *Codonopsis pilosula* -ingredient-target-disease" network

The"*Codonopsis pilosula*-Ingredient-Target-Disease" network was constructed using the Cytoscape 3.7.2 software. Network Analyzer was employed to compute network topological parameters for network analysis.

Hematological analysis

The prothrombin time (PT), thrombin time (TT), activated partial thromboplastin time (APTT), fibrinogen levels (Fib), D-dimer (DD), fibrinogen degradation products (FDP), and antithrombin III (ATIII) in the abdominal aortic blood of rats were measured using the fully automated coagulometer (STAGO-STA-COMLACT).

Enzyme-linked immunosorbent assay (ELISA)

The ELISA assay kits were purchased from Abcam (UK) for the determination of TNF-α (ab236712, Abcam) and IL-10 (ab214566, Abcam) levels in rat serum. The experimental procedures included antibody coating, sample incubation, addition of enzyme-conjugated antibodies, and color development using TMB substrate, followed by the quantification of optical density (OD) at 450 nm wavelength using an ELISA reader. Each experimental assay was performed in triplicate.

Cell culture and transfection

HTR-8/Svneo cells, derived from the human placental chorionic villi (iCell-h390, iCell, Shanghai, China), were cultured in RPMI 1640 medium (11875119, GIBCO, USA) supplemented with 10% fetal bovine serum at 37 °C in a humidified atmosphere containing 5% CO_2 using a CO_2 incubator (51026537, Thermo Fisher, USA). For cell counting, cells were detached using trypsin, the digestion was stopped by adding complete RPMI 1640 medium, and the cells were resuspended by gentle pipetting. A mixture of 10 μL of cell suspension and 10 μL of 0.4% trypan blue dye was loaded into the Countess cell counting chamber (C10228, Invitrogen, USA) and cell numbers were determined using a Countess cell counter (AMQAX2000, Invitrogen, USA).

Cell passaging and subsequent experiments were performed when cell confluence reached approximately 80%. All experiments were conducted using cells at the second passage[21]. For transfection, cells were seeded in cell culture dishes or 6-well plates 24 h before transfection, aiming for a confluence of 70% on the day of transfection. The LAMB1 gene was cloned into the eukaryotic expression vector PCDNA3.1 (V79520, Invitrogen, ThermoFisher Scientific, USA) to obtain the target plasmid oe-LAMB1. Transfection was carried out following the instructions of Lipofectamine 2000 (11668-019, Invitrogen, USA). Post-transfection, the medium was replaced after 6–8 h with fresh culture medium, and cells were further incubated for 48 h before subsequent analyses[21].

The experimental groups included: Control group (PBS + mock), LPS group (PBS + mock + LPS), LPS + Mannose-B-L group (mock + Mannose-B-L + LPS), LPS + Mannose-B-M group (mock + Mannose-B-M + LPS), LPS + Mannose-B-H group (mock + Mannose-B-H + LPS), LPS + Mannose-B-M + oe-LAMB1 group (mock + Mannose-B-M + LPS + oe-LAMB1).Each group was treated with 10 μM (Mannose-B-L), 20 μM (Mannose-B-M), 40 μM (Mannose-B-H), or PBS, along with 50 nM oe-LAMB1/mock transfection for 24 h. Then, cells were induced with 1 μg/mL LPS for 24 h. Afterward, cell samples were collected for subsequent analysis.

Cell proliferation assay using CCK-8

Cell viability was measured according to the instructions of the CCK-8 assay kit (ab228554, Abcam, USA). Cells from each group were seeded at a density of 5×10^3 cells per well in a 96-well culture plate in 100 μL of medium containing 10% FBS. After complete adherence, a blank group (medium only) was set up. Cells were treated with different concentrations of Mannose-B (0, 2.5, 5, 10, 20, 40, 80 μM) for 24 h, followed by the addition of 10 μL CCK-8 solution to each well of the plate and further incubation at 37 °C for 4 h. The absorbance was measured at 450 nm. Each experiment was conducted with 6 replicate wells and repeated independently three times. The proliferation rate was calculated as (experimental group - blank group)/(control group - blank group) for graphical representation.

Transwell experiment

A 50 μL Matrigel solution (Catalog #356234, Corning, USA) was used to coat the Transwell chambers, which were then incubated at 37 °C for 30 min to allow the matrix to solidify. Cells were resuspended in serum-free culture medium and seeded into the upper chamber at a density of 5×10^3 cells per well. The cells were then incubated at 37 °C with 5% CO_2 for 24 h, with the lower chamber containing 600 μL of complete culture medium. After 12 h, the cells beneath the membrane were fixed with 4% paraformaldehyde (Catalog #P1110,

Solarbio, Beijing, China) for 15 min, followed by staining with a 1% crystal violet staining solution (Catalog #G1062, Solarbio, Beijing, China). Random images of the cells were captured using a fluorescence microscope (Olympus IX71, Japan), with six fields counted for each sample.

Scratch healing experiment

Cells at a concentration of 2×10^5 cells/mL were cultured in serum-free medium for 24 h at 37 ℃ with 5% CO_2. A scratch was made using a pipette tip and then fresh medium was replaced. The process of scratch closure was observed for 48 h. The experiment was repeated three times. The average distance between cells was calculated using Image J software.

Detection of target gene expression using RT-qPCR

Tissues and cellular total RNA were extracted using Trizol (catalog number 16096020, Thermo Fisher Scientific, New York, USA). The mRNA was reverse transcribed to cDNA using a reverse transcription kit (catalog number RR047A, Takara, Japan). The reaction system was prepared using the SYBR® Premix Ex TaqTM II kit (catalog number DRR081, Takara, Japan), and real-time qRT-PCR was conducted on a ABI 7500 real-time PCR system (Applied Biosystems, Foster City, CA, USA) with the following program: initial denaturation at 95 °C for 10 min, followed by 35 cycles of denaturation at 95 °C for 15 s, annealing at 60 °C for 30 s, and extension at 72 °C for 45 s. β-Actin was used as the internal control gene. Each qRT-PCR reaction was performed in triplicate, and the experiment was repeated three times. The experimental group to control group ratio of target gene expression was calculated using the $2^{-\Delta\Delta Ct}$ method, where $\Delta\Delta CT = \Delta Ct$ experimental group - ΔCt control group, and $\Delta Ct = Ct_{\text{target gene}} - Ct_{\text{internal reference gene}}$. Ct represents the cycle threshold when the fluorescent signal reaches the set threshold, indicating exponential amplification. Primer details are provided in Table S1.

Western blot

Add RIPA lysis buffer containing PMSF (P0013B, Biyuntian, Shanghai, China) to lyse tissues and extract total proteins from cells. The supernatant is assayed using a BCA protein assay kit (P0011, Biyuntian, Shanghai) to determine the total protein concentration of each sample. Adjust the protein concentration to 1 μg/μL and set the sample volume to 100 μL per tube. Subsequently, boil the samples for 10 min to denature the proteins and store them at −80 °C for later use.

Prepare SDS gels ranging from 8 to 12% based on the target protein band size. Load equal amounts of protein samples into each lane using a microvolume pipette for electrophoretic separation. Transfer the proteins from the gel to a PVDF membrane (1620177, BIO-RAD, USA). Block the membrane with 5% BSA at room temperature for 1 h. Incubate the membrane overnight at 4 °C with rabbit anti-β-Actin (ab8226, 1:1000, Abcam, UK), rabbit anti-LAMB1 (ab108536, 1:1000, Abcam, UK), rabbit anti-TNF-α (ab307164, 1:1000, Abcam, UK), rabbit anti-IFN-γ (NBP2-66900, 1:500, Novus, USA), rabbit anti-IL-4 (66142-1-Ig, 1:1000, Proteintech, Wuhan, China), and rabbit anti-IL-10 (ab9969, 1:1000, Abcam, UK) antibodies. Wash the membrane three times for 5 min each with 1× TBST buffer at room temperature. Incubate with an HRP-conjugated goat anti-rabbit/goat anti-mouse IgG secondary antibody (ab6721/ab6728, 1:1000, Abcam) at room temperature for 1 h. Wash the membrane three times for 5 min each with 1× TBST buffer at room temperature. Submerge the membrane in ECL substrate (1705062, BIO-RAD, USA) and incubate at room temperature for 1 min. Remove excess liquid, cover with plastic wrap, and expose the bands using an Image Quant LAS 4000 C gel imager (GE Company, USA). Normalize the total cellular proteins with β-Actin as an internal control. Calculate the relative protein expression levels by the ratio of the grayscale values of the target bands to the reference β-Actin bands to evaluate the expression levels of various proteins. Repeat each experiment three times.

Data analysis

Statistical analyses in this study were performed using GraphPad Prism 9 software (GraphPad Software, USA). Descriptive statistics are presented as mean ± standard deviation. Prior to hypothesis testing, normality and homogeneity of variances were assessed. When the data met the assumptions of normal distribution and equal variances, between-group comparisons were conducted using unpaired t-tests for two groups and either one-way analysis of variance or repeated measures analysis of variance for multiple group comparisons. $p < 0.05$ indicates that the difference is statistically significant.

Results

Transcriptomic analysis reveals the molecular mechanisms of sch

To delve into the molecular mechanisms directly linked to SCH, we conducted transcriptome sequencing analysis on decidual samples from 12 model group pregnant rats and 12 normal control pregnant rats (Fig. 1A). Initially, we standardized microarray data using normalization methods, and PCA analysis confirmed the successful elimination of batch effects (Fig. 1B). Differential gene analysis revealed 83 significantly DEGs between the model and normal groups, with 44 upregulated and 39 downregulated genes (Fig. 1C). Ranked by the degree of difference, a heatmap of the top 50 upregulated and downregulated genes was generated (Fig. 1D).

GO enrichment analysis indicated that the differential genes primarily participate in BP such as immune response, viral processes, and blood pressure regulation. Particularly, they exhibited distinct functional enrichment in the virus life cycle and host-pathogen interactions. In terms of CC, specific cell structures involving cell projections, microvilli, and apical plasma membrane were implicated. Molecular function analysis unveiled a series of genes associated with endopeptidase activity (Fig. 1E, Table S2). KEGG pathway analysis emphasized the significance of the complement system, metabolic processes, and pathways related to the virus life cycle and signaling pathways. These findings revealed the potential role of nourishing cell layer in immune regulation and

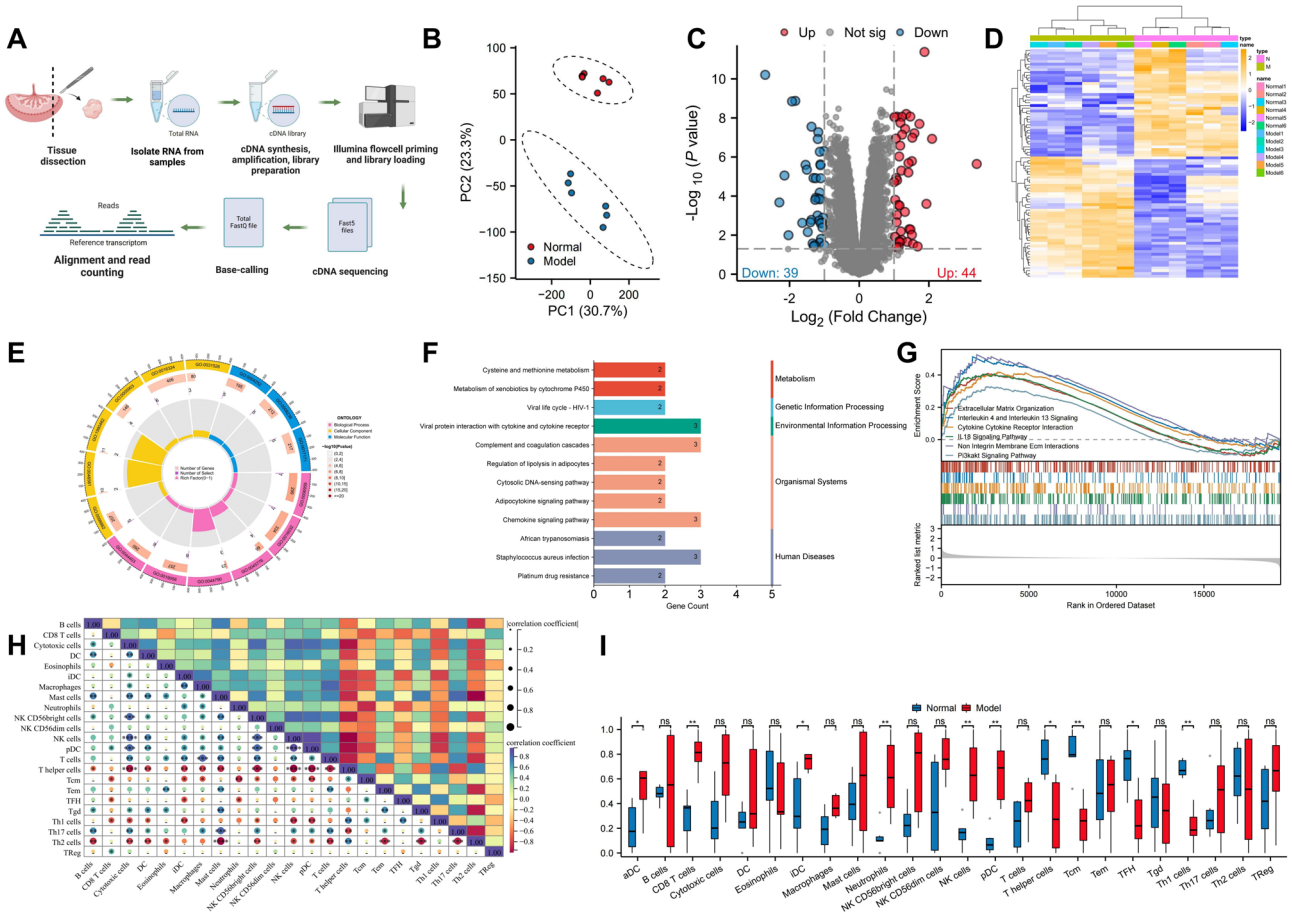

Fig. 1. Differential Transcriptomic and Functional Enrichment Analysis between Normal and Model Groups. Note: (A) Schematic of the transcriptomic sequencing process; (B) PCA of placental tissue samples from the normal control and model groups (Normal = 6, Model = 6) showing pre and post-PCA dimensions with percentages of variance explained in parentheses; (C) Volcano plot of 83 DEGs in placental tissue samples between the normal control and model groups, red dots represent significantly upregulated genes, blue dots represent significantly downregulated genes, and black dots represent genes without differential expression; (D) Heatmap of the top 50 most significantly upregulated and downregulated genes, with yellow indicating high expression and blue indicating low expression; (E) Circular plot of GO functional enrichment analysis of DEGs, where outer to inner layers denote functional categories, total number of genes in each category, number of significantly upregulated genes, and enrichment factors; (F) Enrichment analysis of DEGs in KEGG pathways, listing pathways and the number of enriched genes, categorized by the top six KEGG Pathway classes; (G) Gene Set Enrichment Analysis (GSEA) enrichment analysis of the transcriptome gene expression profile, each line represents a specific gene set with unique colors, upregulated genes are located to the left of the coordinate origin, while downregulated genes are to the right of the x-axis; (H) Heatmap showing the correlation of different immune cell types in normal control and Model samples evaluated using the single-sample Gene Set Enrichment Analysis (ssGSEA) algorithm; (I) Comparison of gene expression levels of immune cell subgroups in normal control and Model samples (Normal = 6, Model = 6). * indicates $p < 0.05$ for inter-group comparison, ** indicates $p < 0.01$, and "ns" indicates no significant difference between the groups.

infection defense (Fig. 1F). GSEA analysis further confirmed significant enrichment of these differential genes in extracellular matrix organization, cytokine signaling, and key signaling pathways like PI3K-Akt (Fig. 1G).

By utilizing the "ssGSEA" algorithm to analyze immune cell infiltration in placental tissue samples from the normal control and model groups, a heatmap illustrated the correlation of 24 immune cell types between the control and model groups (Fig. 1H). The results indicated significant differences in the infiltration levels of various immune cell types (Fig. 1I).

In conclusion, the pathogenesis of SCH is closely associated with alterations in immune cell infiltration, extracellular matrix tissue remodeling, and crucial signaling transduction pathways. These findings elucidate the role of changes in nourishing cell status in regulating pathological processes, providing an essential molecular mechanism foundation for the subsequent development of targeted disease intervention strategies.

Network pharmacology screening of *Codonopsis pilosula* in alleviating subclinical hypothyroidism: candidate genes and chemical components

To identify candidate genes and chemical components capable of alleviating SCH, we conducted network pharmacology screening. Initially, we employed WGCNA to identify key genes involved in the pathogenesis of SCH. We first clustered 6 normal samples and 6 SCH samples, eliminating obvious outliers by setting a threshold (Figure S1A). Subsequently, with $R^2 > 0.7$ and high average connectivity, we set the soft threshold to 11 for further analysis (Figure S1B-C). Hierarchical clustering of genes in the SCH dataset was performed based on the dissimilarity matrix, resulting in the construction of a dendrogram (Fig. 2A). After merging strongly correlated modules with a clustering height limit of 0.25, we identified 4 gene modules for further investigation (Fig. 2B). To screen modules highly correlated with SCH, we conducted PCA of genes within each module, extracting the value of the first principal component as the module eigengene (ME), and assessing the clinical significance of each module based on its correlation with clinical features. Our results revealed a strong positive correlation of the Brown module with SCH ($r = 0.99$, $p = 4e-09$), along with the highest gene importance (Fig. 2C, Figure S1D). The correlation coefficient analysis of each module with SCH is shown in Figure S1E. Subsequently, the core genes of the Brown module were selected for further analysis in this study.

Effective chemical components of *Codonopsis pilosula* were retrieved from the SymMap database, and these components were subjected to screening (Table S3). Subsequently, the target proteins of these chemical components were identified, totaling 1877 targets (Table S4). By intersecting the core genes of the Brown module, transcriptome DEGs, and targets of *Codonopsis pilosula* active components, we identified 9 target genes related to SCH (Fig. 2D), with their expression levels depicted in Fig. 2E. These data were then imported into Cytoscape software to construct a network comprising *Codonopsis pilosula*, active components, targets, and the disease (Fig. 2F). Node analysis of the network revealed Mannose-B to have the most significant degree value (Fig. 2G), being associated with 6 target genes (Fig. 2H).

In conclusion, network pharmacology screening has unveiled potential targets linked to the pathogenesis of SCH in specific components of *Codonopsis pilosula*, with Mannose-B displaying the most significant network connectivity among candidate targets, suggesting its potential importance in the treatment of SCH.

Validation of candidate targets with Mannose-B molecule docking

We conducted molecular docking analysis of candidate proteins with the Mannose-B molecule using software including AutoDockTools 1.5.6 and Vina 1.1.2. Initially, the 2D and 3D chemical structures of Mannose-B were determined using the PubChem database. The specific structures are illustrated in Fig. 3A. Mannose-B was docked with the candidate target proteins LAMB1, ABCC2, ACTA1, CA2, CXCR4, and TRIM15, showing binding affinities of −6.1 kcal/mol, −5.9 kcal/mol, −5.7 kcal/mol, −5.9 kcal/mol, −5.0 kcal/mol, and − 0.1 kcal/mol, respectively (Fig. 3B-G). Simultaneously, we used SPR technology to measure the binding ability of Mannose-B with different candidate proteins (Fig. 3H), and the results showed that Mannose-B had the strongest binding ability with LAMB1, with a binding affinity of 5.64 μM.

Despite LAMB1 having the highest molecular binding free energy, its values were notably close to those of ABCC2, CA2, and ACTA1. To further validate the significance of the target genes and complement the molecular docking data, we prioritized the evaluation of DEGs using the random forest algorithm. Ensuring stability and predictive accuracy of the random forest tree model (Figure S2A-E), we identified significant feature importance of LAMB1 in the random forest analysis (Figure S2F), consistent with its high binding energy observed in the docking. The results from the random forest analysis not only reinforce the findings of molecular docking but also suggest a crucial role of LAMB1 in the drug mechanism, providing a strong bioinformatics basis for our subsequent functional experiments and mechanism studies.

These results demonstrate that, compared to other candidate targets, Mannose-B has a higher binding affinity with LAMB1. Mannose-B can form a stable molecular conformation with LAMB1 and plays a key role in regulating SCH.

Construction of mannose-B-target interaction pharmacophore model

Building upon previous research findings, we utilized the PharmMapper database to analyze the receptor targets and pharmacophore structure of the drug molecule Mannose-B. The results did not directly indicate LAMB1 as a target of Mannose-B, suggesting that LAMB1 might be a novel target warranting further in-depth analysis and verification in future studies. Through Metascape analysis of its receptor targets, we identified their involvement in key BP such as immune response regulation, metabolism, and tumor biology (Figure S3A, Table S5). The core network identified by the MCODE algorithm (MCODE1) revealed the potential role of LAMB1 in extracellular matrix adhesion and cell adhesion pathways (Figure S3B, Table S6). This indicates that Mannose-B may influence LAMB1 through these pathways or target proteins to regulate SCH.

Furthermore, we analyzed the pharmacophore structure of each target in the MCODE1 network and performed an analysis incorporating quantitative characteristics, highlighting the critical properties of these target proteins in drug-target interactions. Among these, ITGAV, being directly connected to LAMB1, showed a leading number of pharmacophore features (Num Feature = 10) and a high Z-score (2.747), indicating strong potential interaction with Mannose-B (Figure S3C-E). Therefore, we speculate that Mannose-B may indirectly regulate LAMB1 through the intermediary molecule ITGAV, thereby modulating the relevant BP of SCH.

In conclusion, while the pharmacophore analysis of Mannose-B did not directly correlate with LAMB1, in-depth network biology analysis revealed the association of LAMB1 with key BP and its potential role in cellular function regulation. This provides a foundation for Mannose-B to indirectly regulate LAMB1 through specific pathways, showcasing a novel approach that integrates network pharmacology and bioinformatics analysis to elucidate the molecular mechanisms behind complex biological effects.

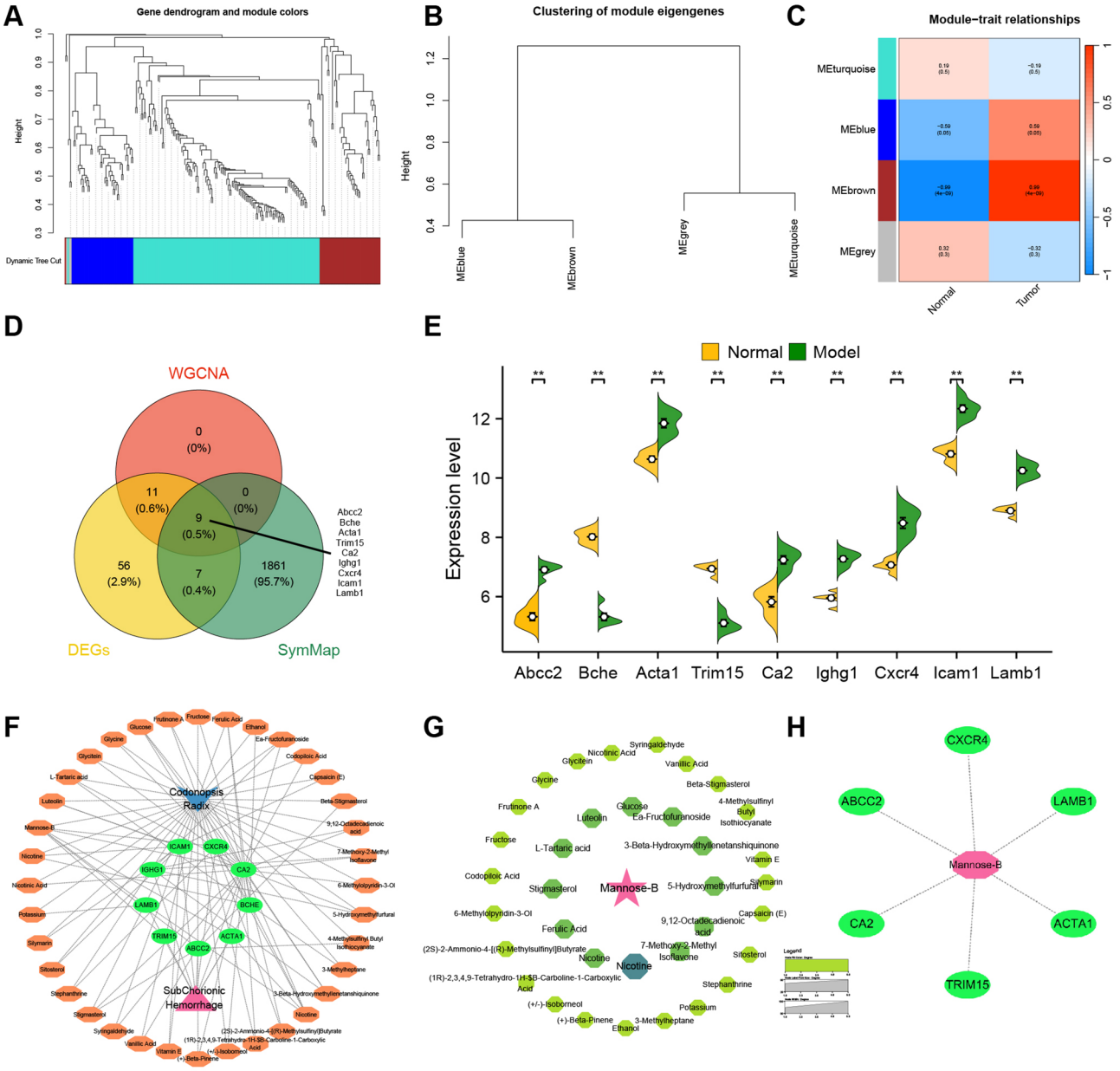

Fig. 2. Construction of Co-expression Network and Traditional Chinese Medicine Network using WGCNA. Note: (A) Hierarchical clustering analysis was conducted to detect co-expression clusters with corresponding color assignments. Each color represents a module in the gene co-expression network constructed by WGCNA; (B) The dendrogram was cut at a height of 0.25 to build four gene expression modules; (C) Heatmap of the correlation coefficients between different modules and traits. Each cell contains the correlation coefficient and corresponding P-value, with red indicating positive correlation and blue indicating negative correlation; (D) Venn diagram of the intersection between characteristic genes of the Brown module identified through WGCNA analysis and DEGs; (E) Differential expression of 9 core genes in the sequencing dataset, ** indicating $p < 0.01$ in intergroup comparisons; (F) Interaction network graph of Codonopsis - Active Ingredients - Targets - Diseases constructed using Cytoscape software. Pink represents diseases, blue represents Codonopsis, cyan oval represents common targets of diseases and drugs, and orange represents active ingredients of Codonopsis; (G) Network graph of active chemical components of Codonopsis obtained from the SymMap database, with node colors arranged based on their degree values; (H) Association diagram between the active ingredient Mannose-B of *Codonopsis pilosula* and its targets.

Mannose-B, an active ingredient of codonopsis radix, alleviates SCH by inhibiting lamb1 expression

Initially, we assessed the mRNA and protein expression of LAMB1 in placental tissues of a rat model using RT-qPCR and Western Blot. Results showed a significant upregulation of LAMB1 mRNA and protein expression

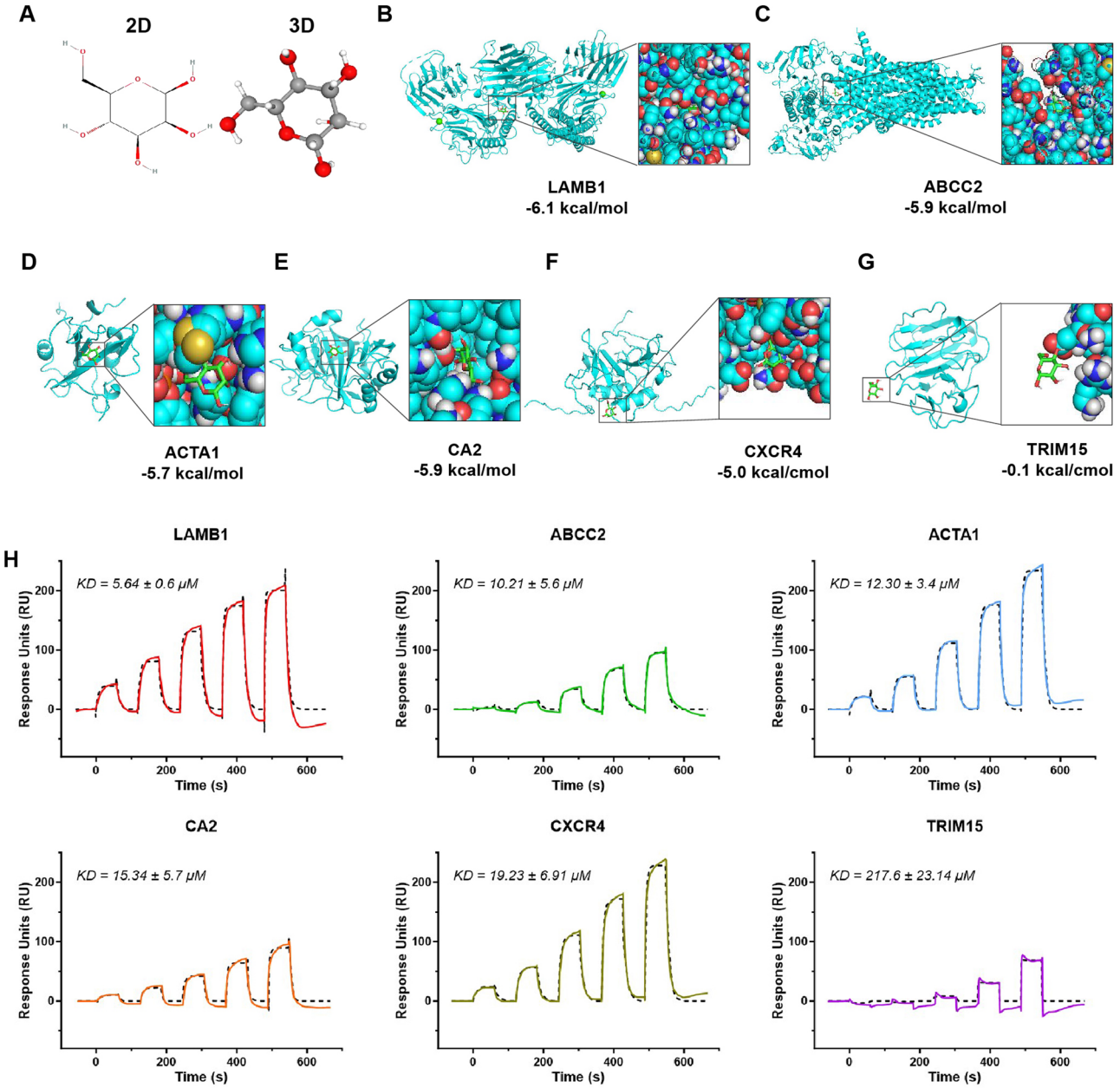

Fig. 3. Molecular Docking of Candidate Targets with Mannose-B. Note: (A) 2D and 3D chemical structures of Mannose-B; (B-G) Interaction status of eight candidate targets with Mannose-B molecule. On the left, the three-dimensional structure of the protein is shown, with blue representing the secondary structure of each target and green indicating the structure of the Mannose-B molecule. On the right, a magnified view of the protein surface is displayed, highlighting the interacting small molecule and its corresponding binding energy; (H) Affinity tests of the six candidate molecules with Mannose-B.

in the Model group compared to the Normal group. Following Mannose-B intervention, LAMB1 expression decreased notably. Moreover, the Model + Mannose-B + oe-LAMB1 group exhibited a significant increase in LAMB1 expression compared to the Model + Mannose-B group (Fig. 4A-B).

Evaluation of clotting parameters in the rat groups showed that compared to the Normal group, the Model group displayed elevated levels of PT), APTT, TT, DD, FDP, and ATIII, while Fib levels decreased. In contrast, the Model + Mannose-B group demonstrated decreased PT, APTT, TT, DD, FDP, and ATIII levels along with increased Fib levels compared to the Model group. Additionally, the Model + Mannose-B + oe-LAMB1 group exhibited increased PT, APTT, TT, DD, FDP, and ATIII levels and decreased Fib levels compared to the Model + Mannose-B group (Fig. 4C-E).

Compared to the Normal group, the Model group rats had smaller fetal body length and placental diameter, reduced litter size, fetal viability, fetal body weight, and placental weight. In comparison to the Model group, the Model + Mannose-B group showed increases in fetal body length and placental diameter, as well as significant

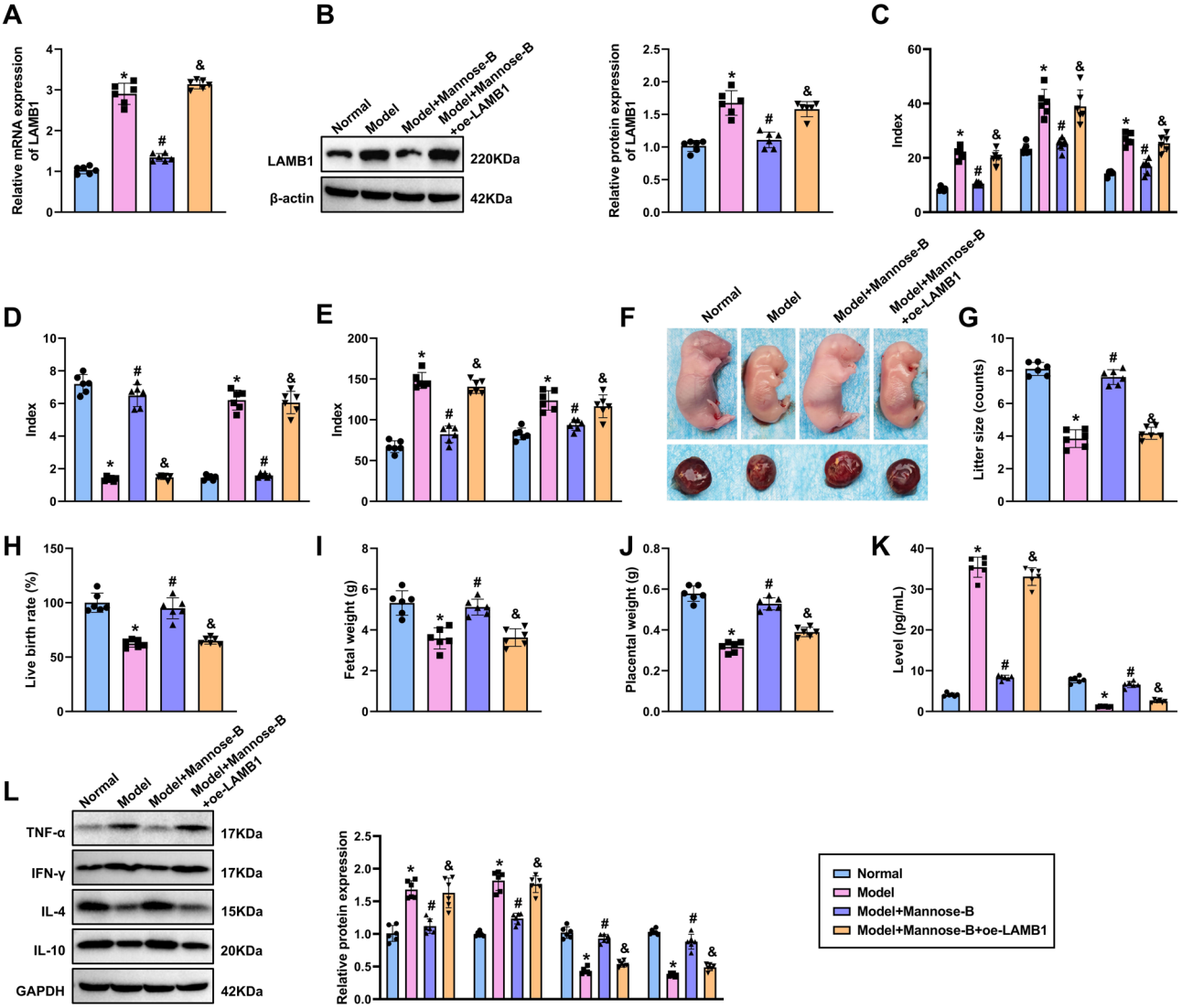

Fig. 4. Impact of Mannose-B Regulation on LAMB1 Expression in SCH. Note: (A-B) Detection of LAMB1 mRNA and protein expression levels in rat placentas in each group via RT-qPCR (A) and Western Blot (B); (C-E) Comparison of coagulation function indicators in rat groups, where PT stands for PT, APTT for APTT, TT for TT, Fib for fibrinogen, DD (D-Dimer) for the marker of thrombus formation and dissolution, FDP for fibrin degradation products, and ATIII for antithrombin III; (F) Morphological comparison of rat fetuses and placentas in each group; (G-J) Statistical analysis of litter size (G), fetal viability rate (H), fetal body weight (I), and placental weight (J) in each group; (K) ELISA detection of TNF-α and IL-10 levels in the serum of pregnant rats in each group; (L) Measurement of protein levels of inflammatory factors TNF-α, IFN-γ, IL-4, and IL-10 in rat placental tissue by Western Blot. * indicates $p < 0.05$ compared to the Normal group, # indicates $p < 0.05$ compared to the Model group, and & indicates $p < 0.05$ compared to the Model + Mannose-B group. Six rats were used in each group.

improvements in litter size, fetal viability, fetal body weight, and placental weight. Conversely, in comparison to the Model + Mannose-B group, the Model + Mannose-B + oe-LAMB1 group exhibited decreased fetal body length and placental diameter, lowered litter size, fetal viability, fetal body weight, and placental weight (Fig. 4F-J).

ELISA analysis of TNF-α and IL-10 levels in serum samples revealed that compared to the Normal group, the Model group rats had significantly increased TNF-α and decreased IL-10 levels. Conversely, the Model + Mannose-B group exhibited decreased TNF-α and increased IL-10 levels compared to the Model group. Furthermore, the Model + Mannose-B + oe-LAMB1 group displayed increased TNF-α and decreased IL-10 levels compared to the Model + Mannose-B group (Fig. 4K). Western Blot analysis of inflammatory-related protein levels in rat placental tissues showed that compared to the Normal group, the Model group displayed a notable increase in pro-inflammatory factors TNF-α and IFN-γ expression, along with a significant decrease in anti-inflammatory factors IL-4 and IL-10 expression. In contrast, the Model + Mannose-B group showed decreased TNF-α and IFN-γ expression and increased IL-4 and IL-10 expression compared to the Model group.

Interestingly, the Model + Mannose-B + oe-LAMB1 group exhibited increased TNF-α and IFN-γ expression and decreased IL-4 and IL-10 expression compared to the Model + Mannose-B group (Fig. 4L).

These results indicate that the active ingredient Mannose-B from Codonopsis Radix may alleviate SCH and inflammatory responses by inhibiting the expression of LAMB1.

Mannose-B promotes proliferation, migration, and invasion of human trophoblast cells through inhibiting LAMB1 expression

Subsequently, we conducted in vitro experiments using human trophoblast cells HTR-8/Svneo to further validate the impact of Mannose-B regulation on LAMB1 expression in HTR-8/Svneo cell functions. Initially, HTR-8/Svneo cells were treated with varying concentrations of Mannose-B (0, 2.5, 5, 10, 20, 40, 80 μM) for 24 h, and the proliferative capacity was assessed using a CCK-8 assay kit. The results demonstrated that treatment with Mannose-B concentrations ranging from 0 to 40 μM for 24 h did not reduce cell viability below 90% of the control group (Fig. 5A). Therefore, 10 μM (Mannose-B-L), 20 μM (Mannose-B-M), and 40 μM (Mannose-B-H) Mannose-B were selected for the dose-response experiment; based on Figure S4, we chose 20 μM Mannose-B as the intervention factor.

Mannose-B was used at 10 μM (Low), 20 μM (Medium), and 40 μM (High) concentrations. Cell proliferation capacity post Mannose-B treatment was evaluated using the CCK-8 assay. The findings illustrated that compared to the Control group, the proliferation capacity of HTR-8/Svneo cells in the LPS group significantly decreased; in contrast, the proliferation capacity of HTR-8/Svneo cells in the LPS + Mannose-B-L/-M/-H group noticeably increased compared to the LPS group; further, compared to the LPS + Mannose-B group, the proliferation capacity of HTR-8/Svneo cells in the LPS + Mannose-B-M + oe-LAMB1 group considerably decreased (Fig. 5B; Figure S4A). To determine whether Mannose-B affects cell invasiveness and migration processes, a scratch assay and Transwell experiment were conducted. The results revealed that compared to the Control group, the migration and invasion abilities of HTR-8/Svneo cells in the LPS group significantly decreased; in contrast, the migration and invasion capacities of cells in the LPS + Mannose-B-L/-M/-H group notably increased in comparison to the LPS group; moreover, the migration and invasion abilities of cells in the LPS + Mannose-B + oe-LAMB1 group significantly decreased compared to the LPS + Mannose-B-M group (Fig. 5C-D; Figure S4B-C).

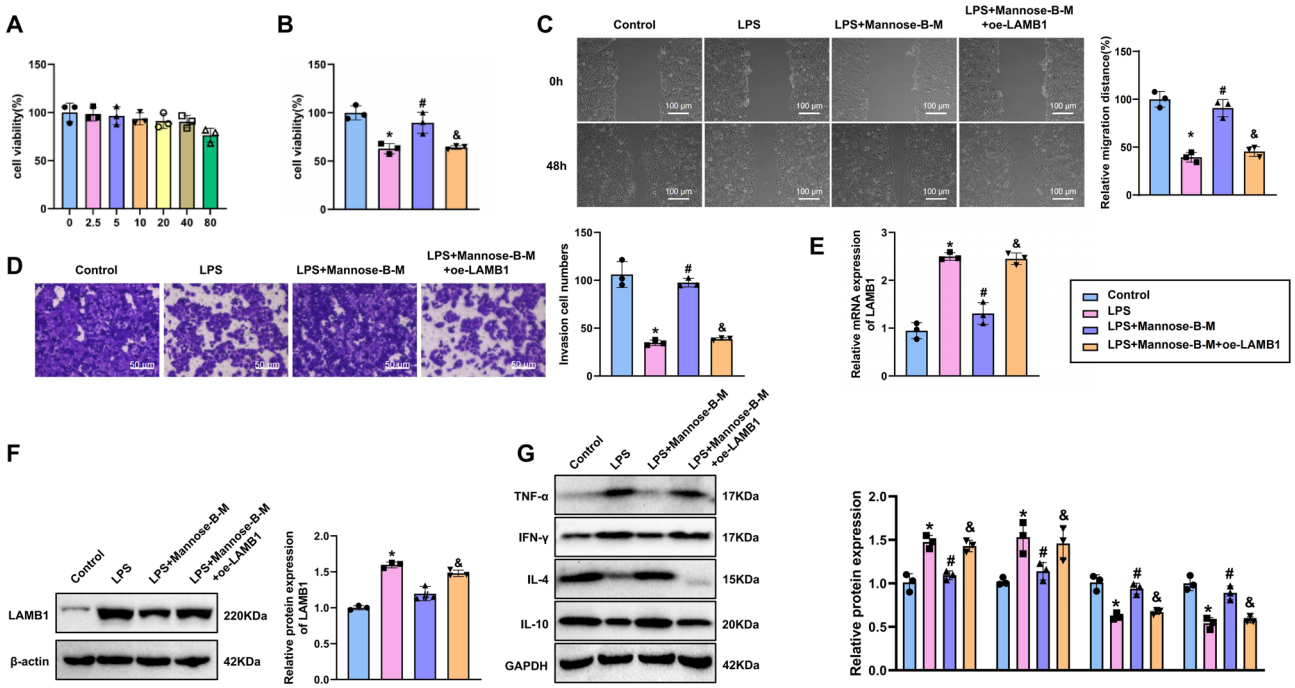

Fig. 5. The Impact of Mannose-B Regulation on LAMB1 Expression on Proliferation, Migration, and Invasion of Human Trophoblast Cells. Note: (A) HTR-8/Svneo cells were treated with different concentrations of Mannose-B for 24 h, and cell viability was measured using the CCK-8 assay; (B) Changes in cell viability of HTR-8/Svneo cells were determined by the CCK-8 assay; (C) Cell scratch assay was performed to assess cell migration of HTR-8/Svneo cells, scale bar: 100 μm; (D) Transwell assay was conducted to evaluate the invasion of HTR-8/Svneo cells, scale bar: 50 μm; (E) RT-qPCR was utilized to measure the mRNA expression of LAMB1 in HTR-8/Svneo cells; (F) Western Blot analysis was employed to determine the protein expression of LAMB1 in HTR-8/Svneo cells; (G) Western Blot analysis was carried out to assess the protein expression of inflammatory factors in HTR-8/Svneo cells. * indicates $p < 0.05$ compared to the Control group, # indicates $p < 0.05$ compared to the LPS group, and & indicates $p < 0.05$ compared to the LPS + Mannose-B group. All cell experiments were repeated three times.

We assessed LAMB1 expression using RT-qPCR and Western Blot analysis and observed that compared to the Control group, the LAMB1 expression in the LPS group notably increased; conversely, the LPS + Mannose-B-L/-M/-H group exhibited reduced LAMB1 expression compared to the LPS group; additionally, the LPS + Mannose-B-M + oe-LAMB1 group showed a marked increase in LAMB1 expression compared to the LPS + Mannose-B-L/-M/-H group (Fig. 5E-F; Figure S4D-E). Similarly, Western Blot analysis of inflammatory markers demonstrated that compared to the Control group, the expressions of TNF-α and IFN-γ significantly increased in the LPS group, while IL-4 and IL-10 expressions notably decreased; further, compared to the LPS group, the LPS + Mannose-B-L/-M/-H group exhibited decreased TNF-α and IFN-γ expressions and increased IL-4 and IL-10 expressions; and compared to the LPS + Mannose-B-L/-M/-H group, the LPS + Mannose-B-M + oe-LAMB1 group displayed increased TNF-α and IFN-γ expressions and decreased IL-4 and IL-10 expressions (Fig. 5G; Figure S4F).

These data demonstrate that Mannose-B promotes the proliferation, migration, and invasion of human trophoblast cells by downregulating LAMB1 expression. Notably, a dose-dependent effect was observed, with the medium concentration (20 μM) exerting the most pronounced impact, suggesting a potential optimal range for its biological activity.

Discussion

Subchorionic Hematoma (SCH), also known as subchorionic bleeding, refers to the bleeding beneath the uterine wall caused by partial detachment of trophoblast cells, leading to the accumulation of blood between the chorionic membrane and the decidua[22]. Although SCH is typically diagnosed through ultrasound examination in the first three months of pregnancy, its potential risks to the mother and fetus are extremely significant. Research shows that SCH is associated with increased rates of miscarriage, preterm birth, and placental abruption, which can have long-term adverse effects on maternal and fetal health[1]. Currently, SCH treatment mainly relies on conservative methods such as rest, avoiding strenuous activity, and regular monitoring, reflecting the limitations of existing treatment strategies, partly due to insufficient understanding of SCH's etiology and molecular mechanisms[23]. Therefore, in-depth research into the specific molecular mechanisms of SCH is essential, as it is critical for the development of more targeted and effective treatments.

In recent years, there has been increasing research on the pharmacology and molecular mechanisms of Traditional Chinese Medicine (TCM) in treating gynecological diseases[24]. Among these, *Codonopsis pilosula* (DangShen) stands out as a traditional herbal medicine with a long history of use. Studies have shown that *Codonopsis pilosula* contains various active components, including polysaccharides, saponins, and certain amino acids, which may have beneficial effects such as improving gastrointestinal protection, replenishing qi and blood, enhancing immunity, anti-fatigue, and potential anti-cancer activities[25,26]. Furthermore, animal studies suggest that *Codonopsis pilosula* extracts may help regulate blood glucose and insulin levels[25]. However, the molecular mechanisms of *Codonopsis pilosula* in treating SCH still need further investigation.

The aim of this study is to investigate the mechanism of action of the active ingredient Mannose-B from *Codonopsis pilosula* in SCH, particularly its impact on the functional changes of human embryonic trophoblast cells through the regulation of LAMB1 expression. SCH is a common and severe complication of pregnancy, typically characterized by the accumulation of blood beneath the uterine lining, which may lead to miscarriage, preterm birth, and other adverse pregnancy outcomes[1,22,27]. Although the exact cause of SCH remains unclear, existing research indicates that abnormal trophoblast cell function plays a crucial role in the initiation and progression of SCH. Through whole transcriptome sequencing and bioinformatics analysis, we identified key genes involved in the pathological process of SCH and utilized network pharmacology to identify effective active components and targets in *Codonopsis pilosula*[28,29]. Experimental results demonstrate that Mannose-B significantly enhances the proliferation, migration, and invasion capabilities of HTR-8/Svneo cells by reducing the expression of LAMB1. Further in vivo experiments validated the inhibitory effect of Mannose-B on LAMB1 expression in rat placenta and its beneficial effects on SCH pathology, offering a fresh perspective on the potential mechanisms of *Codonopsis pilosula* in the treatment of SCH.

In comparison with previous studies, this research systematically reveals for the first time the specific role of Mannose-B in regulating trophoblast cell function. Despite *Codonopsis pilosula* being a TCM with diverse biological activities extensively studied, including anti-inflammatory, antioxidant, and immunomodulatory effects, its precise mechanism of action in pregnancy-related diseases remains unclear. Previous studies have predominantly focused on the impacts of *Codonopsis pilosula* on the immune system and antioxidant capacity, while relatively fewer studies have explored its role in pregnancy complications like SCH[30,31]. Through high-throughput sequencing and bioinformatics analysis, this study elucidated the vital role of LAMB1 in SCH and identified Mannose-B as a crucial component through molecular docking and network pharmacology methods, offering novel scientific evidence for the application of *Codonopsis pilosula* in the treatment of SCH. Additionally, the study elucidates the specific mechanisms of action of Mannose-B in in vitro and in vivo experiments, providing a more comprehensive and detailed understanding of its regulatory effects on cell proliferation, migration, and invasion.

A key finding of this research is that Mannose-B promotes the proliferation, migration, and invasion capabilities of HTR-8/Svneo cells by reducing LAMB1 expression. As a significant member of the laminin family of basement membrane proteins, LAMB1 plays a critical role in extracellular matrix formation and cell migration. Previous studies have indicated that abnormal expression of LAMB1 is closely associated with changes in cellular function in various disease states[32–34]. For instance, in tumor biology, high expression of LAMB1 is closely linked to the invasion and metastasis of tumor cells[14,34]. During pregnancy, LAMB1 also plays a crucial role in the formation and maintenance of the placenta[15,16]. Our research further confirms the high expression of LAMB1 in SCH and its critical role in the pathological process, unveiling for the first time the regulatory effect of Mannose-B on LAMB1, offering a new perspective for understanding the pathological mechanisms of SCH.

Moreover, we discovered that the inhibitory effect of Mannose-B on LAMB1 may be achieved through multiple signaling pathways, providing a direction for further investigation into its specific mechanisms of action.

The study verified the inhibitory effect of Mannose-B on LAMB1 expression and its ameliorative effects on SCH pathological conditions using an SCH rat model. Results demonstrated a significant reduction in LAMB1 expression levels in rat placentas treated with Mannose-B, leading to an improvement in SCH pathology, significantly increasing litter size and viability rate. These findings align with in vitro experiments, further supporting Mannose-B's role in alleviating SCH by modulating LAMB1 expression. Moreover, Mannose-B's beneficial effects on rat coagulation parameters, fetal body weight, and placental weight further validate its potential value in SCH treatment. These discoveries not only confirm our hypothesis but also lay new experimental groundwork for future research. Through detailed in vivo experiments, we not only confirmed the efficacy of Mannose-B but also elucidated its possible mechanisms of action, which hold significant therapeutic implications for SCH treatment.

The inhibitory effect of Mannose-B on LAMB1 expression may involve the regulation of multiple signaling pathways[14,32,34]. Previous studies suggest that LAMB1 plays a crucial role in cell migration and invasion through various signaling pathways such as PI3K/AKT, MAPK, among others[14,35]. Our study, utilizing RT-qPCR and Western Blot techniques, assessed changes in gene and protein expressions, providing initial insights into the potential mechanisms of Mannose-B. Results suggest Mannose-B might suppress key molecules in these pathways, consequently reducing LAMB1 expression and promoting functional recovery of trophoblast cells. This discovery not only reveals specific mechanisms of Mannose-B but also points towards new research directions. Additionally, findings indicate that Mannose-B may influence trophoblast cell functions by modulating other related molecules and signaling pathways, offering further research cues and experimental avenues. Future investigations should delve deeper into the precise mechanisms of Mannose-B, particularly its regulation of various signaling pathways and molecular targets, for a comprehensive understanding of its SCH therapeutic potential.

While this study made significant progress, several limitations exist. Firstly, the specific mechanisms of Mannose-B in in vitro and in vivo experiments require further exploration. Despite our initial exploration of its potential mechanisms, more experimental validations and in-depth analyses are needed. Additionally, this study primarily relied on rat models; however, due to limited research conditions, more human-relevant models were not included. Future research should further verify the effects of Mannose-B in other animal models and clinical samples, such as trophoblast organoids or placental tissue slices. While rat models are crucial for studying human pregnancy-related diseases, differences between rats and humans in physiology and pathology must be carefully considered. Studies have shown that Mannose-B has low absorption efficiency when administered orally, is easily metabolized by the gut microbiota, and is rapidly cleared by the kidneys, with low cellular uptake, leading to low overall bioavailability[36]. Mannose-B's pharmacokinetic behavior is complex, with its absorption and distribution affected by various factors such as administration route, dosage, and individual differences. Its pharmacokinetic characteristics are poor, showing a short half-life, small volume of distribution, and rapid clearance, which limits its sustained action in the body[37]. Furthermore, Mannose-B's metabolic products may interfere with its therapeutic effects[38]. In cancer therapy, Mannose-B may interfere with normal cell glucose metabolism, leading to off-target effects that damage normal tissues, impair immune cell function, and reduce treatment efficacy[39]. Studies suggest that structural modifications could reduce its off-target toxicity[40]. In the future, we can develop novel delivery systems (e.g., nanoparticles, liposomes) to improve bioavailability, optimize pharmacokinetic properties through structural modifications to extend half-life and reduce rapid clearance, and further investigate the molecular mechanisms of off-target effects to develop more selective Mannose-B derivatives.

Although bioinformatics analysis suggests that LAMB1 may be related to downstream signaling pathways like PI3K/AKT and MAPK, there is limited research on this topic. Studies have shown that LAMB1 overexpression decreases the phosphorylation levels of ERK1/2 and SGK1, while knockdown of LAMB1 enhances the phosphorylation levels of ERK1/2 and SGK1[41]; LAMB1 can activate STAT1 during macrophage maturation[42]. In the future, we will further study the mechanisms of LAMB1 in human trophoblast cells, focusing on its interaction with downstream signaling pathways PI3K/AKT and MAPK.

To conclude, this study elucidates, for the first time, the mechanism by which Mannose-B, an active component of Codonopsis, inhibits LAMB1 expression, promoting trophoblast cell proliferation, migration, and invasion to alleviate the pathogenesis of placental abruption. This discovery provides a new theoretical basis for exploring the potential of Codonopsis in SCH intervention. However, the current evidence is limited to in vitro and animal studies. Therefore, the therapeutic potential of Mannose-B in humans remains preliminary, and future studies are needed to confirm its efficacy and safety through well-designed clinical trials before clinical application can be considered. Additionally, investigating other active components in Codonopsis and their synergistic effects will enhance our comprehensive understanding of Codonopsis pharmacology, providing a solid scientific foundation for its modern medical applications. Through these studies, we aim to offer novel treatment strategies for SCH and advance the application of Codonopsis and its active components in modern medicine. Subsequent research should also focus on the effects of Codonopsis in other pregnancy complications, paving the way for new areas of TCM application in modern medicine.

Conclusion

Based on the results above, the active component Mannose-B in *Codonopsis pilosula* may alleviate SCH by modulating the expression of LAMB1, thereby promoting the proliferation, migration, and invasion of human placental trophoblast cells (Fig. 6). This study identified potential active ingredients and targets of *Codonopsis pilosula* for SCH intervention through network pharmacology and provided preliminary evidence suggesting that Mannose-B may influence SCH progression by targeting LAMB1. These findings offer a valuable foundation

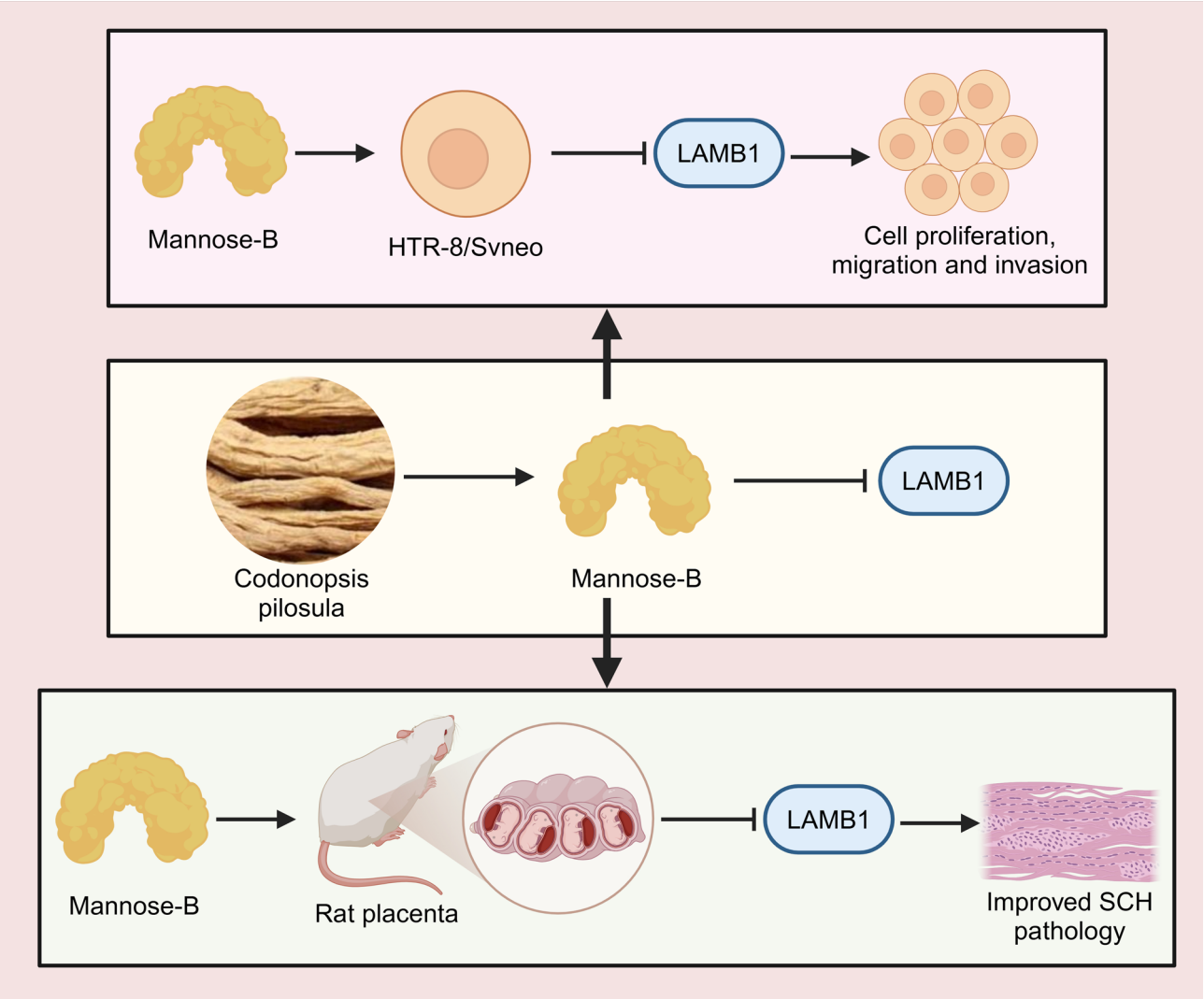

Fig. 6. Investigating the Mechanism of *Codonopsis pilosula* Active Ingredients in Regulating LAMB1 Expression to Impact the Differentiation-Senescence-Apoptosis Balance in Human Trophoblast Cells Using Network Pharmacology and Molecular Docking Techniques.

for future drug development. *Codonopsis pilosula*, as a traditional herbal medicine, has demonstrated safety and efficacy in some human studies in other contexts. However, the role of Mannose-B in treating SCH remains exploratory and is currently supported only by preclinical data. Therefore, further studies are needed to evaluate its efficacy and safety in humans. Moreover, this study primarily focused on the potential regulation of LAMB1 by Mannose-B, while other downstream or parallel molecular mechanisms remain to be investigated. Future research should continue to explore the detailed mechanisms and validate these findings in clinical settings.

Data availability

The data supporting the findings of this study are available at Zenodo with the DOI: 10.5281/zenodo.14557392 (https://doi.org/10.5281/zenodo.14557392).The sequencing data generated in this study have been deposit ed in the NCBI Sequence Read Archive (SRA) under the BioProject accession number PRJNA1287260. The raw sequencing data are available under the following SRA accession numbers: Control group: SRR34390150, SRR34390149, SRR34390146, SRR34390145, SRR34390144, SRR34390143Case group: SRR34390142, SRR34390141, SRR34390140, SRR34390139, SRR34390148, SRR34390147All data are publicly accessible and can be downloaded from the NCBI SRA database.

Received: 10 December 2024; Accepted: 28 July 2025
Published online: 11 August 2025

References

1. Yan, X. et al. Subchorionic hematoma and risk of preterm delivery: a systematic review and meta-analysis. *Am. J. Obstet. Gynecol. MFM*. **5**, 100791 (2023).
2. Naz, S., Irfan, S., Naru, T. & Malik, A. Subchorionic hematoma and pregnancy outcomes in patients with threatened miscarriage. *Pakistan J. Med. Sciences* **38** (2022).
3. Elmas, B. et al. Do First-Trimester subchorionic hematomas affect pregnancy outcomes?? *Z. Für Geburtshilfe Und Neonatologie*. **227**, 31–35 (2022).
4. Chen, Y., Yu, C., Hu, F., Zhu, Y. & Xie, X. Astragalus polysaccharides combined with Codonopsis pilosula polysaccharides modulates the physiological characteristics of trophoblasts via miR-92a-1-5p/CCR7 axis. *Tissue Cell.* **77**, 101827 (2022).
5. Jovanović Krivokuća, M., Vilotić, A., Stefanoska, I., Bojić-Trbojević, Ž. & Vićovac, L. Macrophage migration inhibitory factor in human early pregnancy events and association with placental pathologies. *Placenta* **116**, 51–57 (2021).
6. Yue, J. et al. Characterization of Codonopsis pilosula subsp. Tangshen plastome and comparative analysis of Codonopsis species. *PLOS ONE*. **17**, e0271813 (2022).
7. Li, N., Yang, C., Xia, J., Wang, W. & Xiong, W. Molecular mechanisms of Codonopsis pilosula in inhibiting hepatocellular carcinoma growth and metastasis. *Phytomedicine* **128**, 155338 (2024).
8. Wang, X. et al. Codonopsis pilosula water extract delays D-galactose-induced aging of the brain in mice by activating autophagy and regulating metabolism. *J. Ethnopharmacol.* **327**, 118016 (2024).
9. Yue, J., Xiao, Y. & Chen, W. Insights into genus codonopsis: from past achievements to future perspectives. *Crit. Rev. Anal. Chem.* **54**, 3345–3376 (2023).
10. Li, G. et al. Screening of Codonopsis radix Polysaccharides with Different Molecular Weights and Evaluation of Their Immunomodulatory Activity In Vitro and In Vivo. *Molecules* vol. 27 5454 (2022).
11. Liu, M. et al. Structural characterization, antioxidant activity, and the effects of Codonopsis pilosula polysaccharides on the solubility and stability of flavonoids. *J. Pharm. Biomed. Anal.* **229**, 115368 (2023).
12. Li, N. et al. Isolation, purification, and structural characterization of polysaccharides from Codonopsis pilosula and their Anti-Tumor bioactivity by Immunomodulation. *Pharmaceuticals (Basel)*. **16**, 895 (2023).
13. Zhang, W. et al. Mannose treatment: A promising novel strategy to suppress inflammation. *Front. Immunol.* **12**, 756920 (2021).
14. Lee, H. et al. Upregulation of LAMB1 via ERK/c-Jun axis promotes gastric cancer growth and motility. *Int. J. Mol. Sci.* **22**, 626 (2021).
15. Gorman, B. R. et al. A multi-ancestry GWAS of Fuchs corneal dystrophy highlights the contributions of laminins, collagen, and endothelial cell regulation. *Commun. Biol.* **7**, 418 (2024).
16. Arutyunyan, A. et al. Spatial multiomics map of trophoblast development in early pregnancy. *Nature* **616**, 143–151 (2023).
17. Percie du Sert. The ARRIVE guidelines 2.0: updated guidelines for reporting animal research. *Br. J. Pharmacol.* **177**, 3617–3624 (2020).
18. Han, X. et al. Stimulation of α7 nicotinic acetylcholine receptor by nicotine suppresses decidual M1 macrophage polarization against inflammation in Lipopolysaccharide-Induced Preeclampsia-Like mouse model. *Front. Immunol.* **12**, 642071 (2021).
19. Fang, M. et al. Transfection of Sox11 plasmid alleviates ventilator-induced lung injury via Sox11 and FAK. *Biochem. Biophys. Res. Commun.* **512**, 182–188 (2019).
20. Xue, P. et al. Single Administration of Ultra-Low-Dose Lipopolysaccharide in Rat Early Pregnancy Induces TLR4 Activation in the Placenta Contributing to Preeclampsia. *PLOS ONE* vol. 10 e0124001 (2015).
21. Li, B. et al. NLRP7 deubiquitination by USP10 promotes tumor progression and tumor-associated macrophage polarization in colorectal cancer. *Journal Experimental & Clin. Cancer Research* **40** (2021).
22. Bondick, C. P., Das, J. M. & Fertel, H. *Subchorionic Hemorrhage. In StatPearls* (StatPearls Publishing, 2023).
23. Tuuli, M. G., Norman, S. M., Odibo, A. O., Macones, G. A. & Cahill, A. G. Perinatal outcomes in women with subchorionic hematoma. *Obstet. Gynecol.* **117**, 1205–1212 (2011).
24. Xu, L. et al. Zishen Yutai pill as an adjuvant therapy in threatened miscarriage:a meta-analysis of 23 randomized controlled trials. *Heliyon* **9**, e16213 (2023).
25. Gao, S. M. et al. Traditional uses, phytochemistry, Pharmacology and toxicology of codonopsis: A review. *J. Ethnopharmacol.* **219**, 50–70 (2018).
26. Bailly, C. Anticancer properties of lobetyolin, an essential component of radix Codonopsis (Dangshen). *Nat. Prod. Bioprospecting.* **11**, 143–153 (2020).
27. Pagan, M., Monson, J., Strebeck, R., Edwards, S. & Magann, E. F. Subchorionic hemorrhage in the second and third trimesters of pregnancy: A review. *Obstet. Gynecol. Surv.* **77**, 745–752 (2022).
28. West, B. T. et al. Factors associated with subchorionic hematoma formation in pregnancies achieved via assisted reproductive technologies. *J. Assist. Reprod. Genet.* **37**, 305–309 (2020).
29. Liu, Y., Tong, A. & Qi, X. A large subchorionic hematoma in pregnancy. *Medicine* vol. 99 e20280 (2020).
30. Sun, M. et al. Preparation, characterization and immune activity of Codonopsis pilosula polysaccharide loaded in chitosan-graphene oxide. *Int. J. Biol. Macromol.* **221**, 1466–1475 (2022).
31. Chen, S. et al. Codonopsis lanceolata polysaccharide ameliorates high-fat diet induced-postpartum hypogalactia via stimulating prolactin receptor-mediated Jak2/Stat5 signaling. *Int. J. Biol. Macromol.* **259**, 129114 (2024).
32. Li, Z. Z. et al. Extracellular matrix protein laminin β1 regulates pain sensitivity and anxiodepression-like behaviors in mice. *Journal Clin. Investigation* **131** (2021).
33. Liu, T. et al. RNA helicase DDX24 stabilizes LAMB1 to promote hepatocellular carcinoma progression. *Cancer Res.* **82**, 3074–3087 (2022).
34. Ran, T. et al. LAMB1 is related to the T stage and indicates poor prognosis in gastric cancer. *Technology Cancer Res. & Treatment* **20** (2021).
35. He, W., Zhang, H., Cheng, H., Wen, J. & Li, D. PIK3CD correlates with prognosis, epithelial–mesenchymal transition and tumor immune infiltration in breast carcinoma. *Discover Oncology* **14** (2023).
36. Maciel, L., de Oliveira, D. F., Monnerat, G., Campos de Carvalho, A. C. & Nascimento, J. H. M. Exogenous 10 kDa-Heat Shock Protein Preserves Mitochondrial Function After Hypoxia/Reoxygenation. *Frontiers Pharmacology* **11** (2020).
37. Gao, M. et al. Effect of Glyceryl Monocaprylate–Modified Chitosan on the intranasal absorption of insulin in rats. *J. Pharm. Sci.* **108**, 3623–3629 (2019).
38. Berardi, A., Castells-Graells, R. & Lomonossoff, G. P. High stability of plant-expressed virus-like particles of an insect virus in artificial gastric and intestinal fluids. *Eur. J. Pharm. Biopharm.* **155**, 103–111 (2020).
39. Harada, Y. Manipulating mannose metabolism as a potential anticancer strategy. *FEBS J.* **292**, 1505–1519 (2025).
40. Lustig, R. H. et al. Obesity I: overview and molecular and biochemical mechanisms. *Biochem. Pharmacol.* **199**, 115012 (2022).
41. Yang, Y. C., Ma, Y. L., Liu, W. T. & Lee, E. H. Laminin-β1 impairs Spatial learning through Inhibition of ERK/MAPK and SGK1 signaling. *Neuropsychopharmacology* **36**, 2571–2586 (2011).
42. Tai, D. J. C., Hsu, W. L., Liu, Y. C., Ma, Y. L. & Lee, E. H. Y. Novel role and mechanism of protein inhibitor of activated STAT1 in Spatial learning. *EMBO J.* **30**, 205–220 (2010).

Acknowledgements
The mass spectrometry proteomics data have been deposited to the ProteomeXchange Consortium via the PRIDE partner repository with the dataset identifier PXD059213.

Author contributions
Q.S, Y.G, K.A and J.J conceived and designed the research. XY.W and JJ.X performed the experiments. S.W and Y.Z interpreted the results of the experiments. BY.Z and MW.S analyzed the data. W.F prepared the figures. J.R and W.Y drafted the paper. S.L and C.H or W.Y edited and revised the manuscript. All authors read and approved the final version of the manuscript.

Funding
This study was supported by Open Project of Jiangsu Key Laboratory of Active Molecular Screening of Marine Drugs (No. HY202204), Scientific Research Project on Maternal and Child Health in Lianyungang City (No. F202103), Scientific Research Project on Maternal and Child Health in Lianyungang City (No. F202310), Special Project on Promoting Scientific and Technological Innovation in Xuzhou City in 2022 (Key Research and Development Program (Social Development) - Standardized Treatment of Key Diseases) (No. KC22096), Key Talents in Maternal and Child Health Care in Lianyungang City (No. FRC202003), Jiangsu Province Maternal and Child Health Research Program (No. F202317), Supporting Project of the First People's Hospital of Lianyungang (NO. YK202303) and Supporting Project of the First People's Hospital of Lianyungang (NO. BB202411).

Declarations

Competing interests
The authors declare no competing interests.

Ethical statement
All animal experiments in this study were conducted in accordance with the ARRIVE 2.0 guidelines (Animal Research: Reporting of In Vivo Experiments) 17 and strictly adhered to the animal welfare regulations of China. The experimental protocol was approved by the Jiangsu Ocean University Experimental Animal Ethics Committee (No. Jou2022121107). All procedures were designed to optimize animal welfare and minimize suffering throughout the study.

Additional information
Supplementary Information The online version contains supplementary material available at https://doi.org/10.1038/s41598-025-13918-z.

Correspondence and requests for materials should be addressed to C.H., S.L. or W.Y.